Available online at www.sciencedirect.com

ScienceDirect

IFAC Papers Online CONFERENCE PAPER ARCHIVE

IFAC PapersOnLine 55-37 (2022) 68–73

Reduced Order Modeling of an Autorotating Samara for Steady-State and Dynamic Analysis ⋆

Jonathan McConnell * **Tuhin Das** **

* *University of Central Florida, 4000 Central Florida Blvd, Orlando, FL 32816 (e-mail: jonathan.mcconnell@knights.ucf.edu).*

** *University of Central Florida, 4000 Central Florida Blvd, Orlando, FL 32816 (e-mail: tuhin.das@ucf.edu)*

Abstract: This paper presents a reduced order model for describing the steady-state and dynamic behavior of a single-winged samara seed pod undergoing autorotative descent. Blade Element Theory is employed to capture the span-wise behavior of a samara. By neglecting lateral motion of the center of mass and prescribing a roll angle, a simplified and compact model is developed while retaining reasonable accuracy in comparison to experimental data published in the literature. Steady-state results confirm the validity of assuming a small roll angle, which helps reduce model complexity. Simulation of the dynamics yields reasonable transient behavior and convergence to equivalent steady-state values. Accuracy of the reduced order model suggests the plausibility of designing and controlling simple autorotative mechanisms.

Keywords: Aerodynamics, Autorotation, Bio-inspired motion, Dynamics, Model validation

1. NOMENCLATURE

C_D	Coefficient of drag
C_{D_0}	Additional drag effects
C_L	Coefficient of lift
F	Net force
g	Acceleration due to gravity
I	Moment of inertia
m	Mass
M	Net moment
r	Radial position
R	Blade radius
v_0	Vertical velocity of samara
w	Blade width
α	Local angle of attack
θ	Pitch angle
λ	Tip speed ratio
ρ	Air density
ϕ	Yaw angle
χ	Span ratio
ψ	Roll angle
ω	Angular velocity

2. INTRODUCTION

A samara is a seed pod configuration that naturally autorotates during descent. This increases the distances seeds can be scattered by a single organism, as longer descent times allow for more influence from prevailing winds and gusts, Burrows (1975); Augspurger (1986); Augspurger and Franson (1987); Green (1980); Green and Johnson (1990, 1993). This design also allows for the adoption of larger seeds, as the lower terminal velocity reduces the force of impact substantially. Analyzing the behavior of these naturally evolved rotorcraft can provide valuable insight into the dynamics and design of larger and more sophisticated aerodynamic mechanisms as well as simple micro-rotorcraft. This paper will give focus to samaras of the single-winged variety.

A seminal work by Norberg (1973) has presented a thorough qualitative and experimental analysis of samara stability. Additional literature presents the comparison of samara performance to windmills and parachutes, Hertel (1966); Holden (2016). However, dynamic modeling can provide insight into the transient behavior of samara descent. Furthermore, producing a mathematical model of a samara allows for exploration of the size and samara design conditions which produce stable autorotation. A simple mathematical analysis of samara stability was presented in Ulrich et al. (2010) for the purpose of modeling and controlling a powered single-winged rotorcraft. This work was further expanded upon in Ulrich and Pines (2012). Computational fluid dynamics was utilized in Lentink et al. (2009) and Holden (2016) to analyze the micro-scale effects of turbulence and leading edge vortices. Discussion of the effects of leading edge vortices and the robustness of samara stability to gusts has been given in Limacher (2015). An extensive and detailed model of samara dynamics and an analysis of stability have been presented by Rosen and Seter (1991); Seter and Rosen (1992), which employ Blade Element Method with special attention to the effects of low Reynolds number. Samara experimentation has been conducted by Hertel (1966); Green (1980); Rosen and Seter (1991); Yasuda and Azuma (1997); Nathan et al. (1996); Holden (2016). It is the goal of this paper to provide a reduced order Blade Element model for a samara in vertical descent by neglecting lateral movement and assuming negligible roll angle. This model

⋆ This work was supported by the National Science Foundation, Award #1762986

10.1016/j.ifacol.2022.11.163

will be explored for analysis of both steady-state, and transient behavior. A reduced order model provides many benefits to the prospect of design and control of simple single-winged rotorcraft similar to that of Ulrich et al. (2010); Ulrich and Pines (2012).

3. DYNAMIC MODEL

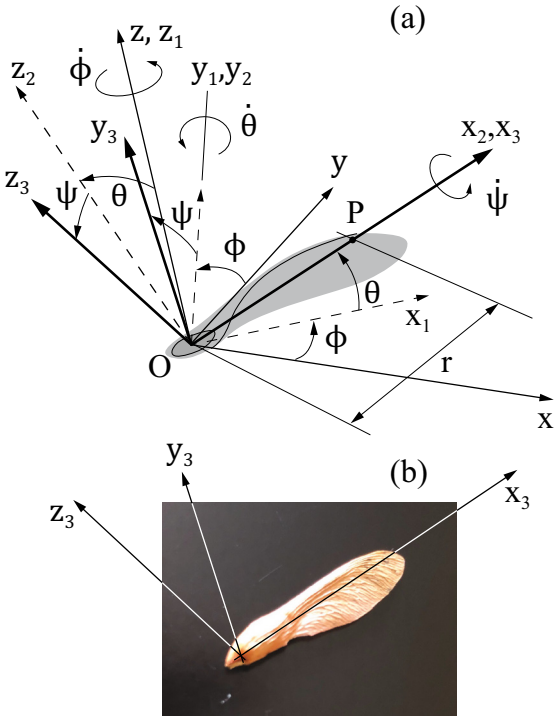

Fig. 1. Euler angle definition for a samara

The equations of motion with respect to a body fixed reference frame are displayed in (1) and (2).

$$\begin{aligned} I_{x_3x_3}\,\dot{\omega}_{x_3} + (I_{z_3z_3} - I_{y_3y_3})\omega_{y_3}\,\omega_{z_3} &= M_{x_3} \\ I_{y_3y_3}\,\dot{\omega}_{y_3} + (I_{x_3x_3} - I_{z_3z_3})\omega_{x_3}\,\omega_{z_3} &= M_{y_3} \\ I_{z_3z_3}\,\dot{\omega}_{z_3} + (I_{y_3y_3} - I_{x_3x_3})\omega_{x_3}\,\omega_{y_3} &= M_{z_3} \end{aligned} \tag{1}$$

$$\begin{aligned} m\dot{v}_0 = &- mg + F_{x_3}\,sin\,\theta \\ &+ F_{y_3}\,sin\,\psi\,cos\,\theta + F_{z_3}\,cos\,\psi\,cos\,\theta \end{aligned} \tag{2}$$

where $I_{x_3x_3}$, ω_{x_3}, and M_{x_3} refer to the moment of inertia, angular velocity, and net moment about the body-fixed x-axis, and F_{x_3} refers to the net force in the direction of the body fixed x-axis. The same naming convention follows for the body-fixed y- and z-axes. The angular velocity of the samara in the body-fixed frame (x_3, y_3, z_3) can be expressed using the Euler angles as follows,

$$\begin{aligned} \boldsymbol{\omega} &= \omega_{x_3}\hat{i} + \omega_{y_3}\hat{j} + \omega_{z_3}\hat{k} \\ &= \left(\dot{\psi} + \dot{\phi}\sin\theta\right)\hat{i} + \left(\dot{\phi}\cos\theta\sin\psi - \dot{\theta}\cos\psi\right)\hat{j} \\ &\quad + \left(\dot{\phi}\cos\theta\cos\psi + \dot{\theta}\sin\psi\right)\hat{k} \end{aligned} \tag{3}$$

The forces F_{x_3}, F_{y_3}, F_{z_3} and the moments M_{x_3}, M_{y_3}, M_{z_3} are due to aerodynamics. To determine them, we start with the position and velocity of a point P shown in Fig. 1(a), expressed relative to O as given below,

$$\begin{aligned} \mathbf{r_P} = \mathbf{r_O} + r\hat{i}, \quad \mathbf{v_P} = \mathbf{v_O} + \left(\boldsymbol{\omega} \times r\hat{i}\right) \\ \mathbf{v_O} = v_o\left(\sin\theta\hat{i} + \cos\theta\cos\psi\hat{j} + \cos\theta\sin\psi\hat{k}\right) \end{aligned} \tag{4}$$

In (4) we have assumed that the point O of the samara has motion predominantly in the vertical direction with

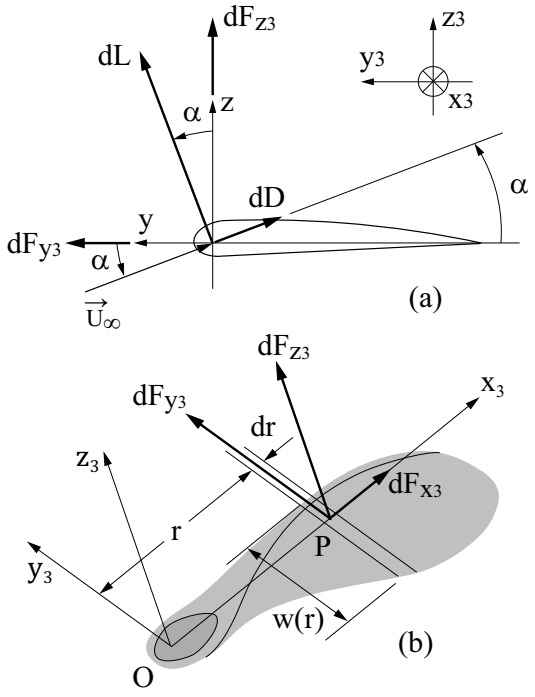

Fig. 2. Elemental forces on a blade

negligible motion in lateral directions. From (3) and (4) we have,

$$\begin{aligned} \mathbf{v_P} =& \mathbf{v_O} + \left(\boldsymbol{\omega} \times r\hat{i}\right) \\ =& v_o\sin\theta\hat{i} + \left[v_o\cos\theta\cos\psi - r\left(\dot{\phi}\cos\theta\sin\psi - \dot{\theta}\cos\psi\right)\right]\hat{k} \\ &+ \left[v_o\cos\theta\sin\psi + r\left(\dot{\phi}\cos\theta\cos\psi + \dot{\theta}\sin\psi\right)\right]\hat{j} \end{aligned} \tag{5}$$

The wind velocity relative to P is $\mathbf{v_{w/P}} = -\mathbf{v_P}$. From Fig. 2 for an element along the samara blade, the local drag and lift forces, dD and dL respectively, are given by

$$\begin{aligned} dD &= \frac{1}{2}\rho w(r)drC_D(\alpha)\|\boldsymbol{U}_\infty\|^2, \\ dL &= \frac{1}{2}\rho w(r)drC_L(\alpha)\|\boldsymbol{U}_\infty\|^2 \end{aligned} \tag{6}$$

where α is the span-wise local angle of attack and from (5),

$$\boldsymbol{U}_\infty = -v_{P,y}\hat{j} - v_{P,z}\hat{k} \quad \text{and} \quad \tan\alpha = -\frac{v_{P,z}}{v_{P,y}} \tag{7}$$

The element forces in body-fixed y_3 and z_3 directions are:

$$\begin{aligned} dF_{y_3} &= \frac{1}{2}\rho w(r)\|\boldsymbol{U}_\infty\|^2\left(\sin\alpha\,C_L(\alpha) - \cos\alpha\,C_D(\alpha)\right)dr \\ dF_{z_3} &= \frac{1}{2}\rho w(r)\|\boldsymbol{U}_\infty\|^2\left(\cos\alpha\,C_L(\alpha) + \sin\alpha\,C_D(\alpha)\right)dr \end{aligned} \tag{8}$$

The overall forces and moments are:

$$\begin{aligned} F_{y_3} = \int_{r_0}^{r_f} dF_{y_3}, \quad F_{z_3} = \int_{r_0}^{r_f} dF_{z_3}, \\ M_{z_3} = \int_{r_0}^{r_f} r\,dF_{y_3}, \quad M_{y_3} = -\int_{r_0}^{r_f} r\,dF_{z_3} \end{aligned} \tag{9}$$

In (9), note that the limits of integration r_0 and r_f are not equal to 0 and R respectively. This is because, as evident from Fig. 1(b), the wing-span that contributes to the aerodynamic forces starts from $r_0 > 0$ and ends at an $r_f < R$. The bottom boundary of r_0 is taken to account for

losses due to the rounded seed geometry near the center of mass, whereas the top boundary of r_f is taken to account for tip losses. In this paper we have assumed constant values of these parameters based on visual inspection. Also, as we resolve the forces and moments we make the following two simplifying assumptions:

(1) We neglect the effect of dF_{x_3}, the elemental force along the blade span. Thus, we assume $F_{x_3} \approx 0$ and neglect its effect on the aerodynamics. This simplifies the dynamic model. The assumption can be removed by using the net relative wind velocity on the (x_3, y_3) plane and accordingly considering blade elements to be tilted from the y_3 axis instead of being parallel to it, as shown in Fig. 2(b).
(2) We assume the rolling moment $M_{x_3} \approx 0$. This is based on the observation that the samara's motion is dominated by the yaw rate $\dot{\phi}$, the pitching motion $\theta, \dot{\theta}$ (coning) and the vertical motion v_0.

A samara is typically an elongated and planar rigid body. Thus, for simplicity we can assume that $I_{z_3z_3} = I_{x_3x_3} + I_{y_3y_3}$. Moreover, due to the slender thickness and planform of the samara blade, it is assumed that the moment of inertia with respect to the spanwise axis, $I_{x_3x_3} \ll I_{y_3y_3}, I_{z_3z_3}$. Accordingly, in this paper we assume, $I_{x_3x_3} = 0$ and $I_{z_3z_3} = I_{y_3y_3}$. It is important to note that the mass of the samara is not evenly distributed. A majority of its mass is concentrated at the seed, at point O (see Fig. 1(a) and (b)). It is imperative that this be taken into consideration when approximating the value for $I_{y_3y_3}$. The resulting reduced moment of inertia helps in achieving coning angles that correlate well with data published in the literature, Norberg (1973). For the purposes of producing a simplified model, the center of mass is taken to be at O.

Through observation of a samara in descent, it is seen that the roll angle, ψ, remains small. With this observation, and consideration to the symmetry of the samara's airfoil profile, it is reasonable to assume that the angle ψ will be nearly if not exactly zero at steady state. Further, the assumption of $M_{x_3} \approx 0$ along with $I_{x_3x_3} = 0$ and $I_{z_3z_3} = I_{y_3y_3}$ implies that the first equation of (1) is identically zero. The dynamics and statics of the system can be studied for different constant values of ψ. Statics analysis reveals that only a small range of ψ around zero is allowable. This simplification reduces the statics problem to that of determining 3 unknowns, namely $\dot{\phi}$, θ, and v_0. The dynamics reduces to 4 states, namely, $\dot{\phi}$, $\dot{\theta}$, θ, and v_0. The simplified dynamics of an autorotating samara is next provided. From the second and third equations of (1), from (2), and imposing $\dot{\psi} = 0$ on ω_{x_3}, ω_{y_3}, ω_{z_3} in (3), we have,

$$\begin{aligned}
\ddot{\theta}\cos\psi + \dot{\phi}^2 \sin\theta\cos\theta\cos\psi + 2\dot{\phi}\dot{\theta}\sin\theta\sin\psi \\
-\ddot{\phi}\cos\theta\sin\psi = -M_{y_3}/I_{y_3y_3} \\
\ddot{\theta}\sin\psi + \dot{\phi}^2 \sin\theta\cos\theta\sin\psi - 2\dot{\phi}\dot{\theta}\sin\theta\cos\psi \\
+\ddot{\phi}\cos\theta\cos\psi = M_{z_3}/I_{y_3y_3} \\
\dot{v}_0 = -g + (F_{y_3}\cos\theta\sin\psi)/m + (F_{z_3}\cos\theta\cos\psi)/m
\end{aligned} \tag{10}$$

where M_{y_3}, M_{z_3} and F_{z_3} are nonlinear functions of the state variables, as given in (8) and (9). It is noted here from (5), (6), and (7) that,

$$\begin{aligned}
\|U_\infty\|^2 &= r^2\dot{\phi}^2\cos^2\theta + (r\dot{\theta} + v_0\cos\theta)^2 \\
\sin\alpha &= [-v_0\cos\theta\cos\psi + r(\dot{\phi}\cos\theta\sin\psi - \dot{\theta}\cos\psi)]/\|U_\infty\| \\
\cos\alpha &= [v_0\cos\theta\sin\psi + r(\dot{\phi}\cos\theta\cos\psi + \dot{\theta}\sin\psi)]/\|U_\infty\|
\end{aligned} \tag{11}$$

4. CONDITIONS FOR STEADY AUTOROTATION

Conditions for steady autorotation can now be derived from the dynamic model above by imposing $\ddot{\theta} = \ddot{\phi} = \dot{\theta} = \dot{v}_0 = 0$. It is noted here, that in deriving the conditions for steady autorotation, we allow the roll angle ψ to assume non-zero constant values. We treat ψ as an input in determining the possible set of autorotational equilibria. The exercise confirms that feasible steady values of ψ lie only a few degrees around $\psi = 0$. The equations for steady autorotation, obtained from (1), (2) and (3) are:

$$\begin{aligned}
\dot{\phi}^2\sin\theta\cos\theta\cos\psi &= -M_{y_3}/I_{y_3y_3} \\
\dot{\phi}^2\sin\theta\cos\theta\sin\psi &= M_{z_3}/I_{y_3y_3} \\
mg &= F_{y_3}\sin\psi\cos\theta + F_{z_3}\cos\psi\cos\theta
\end{aligned} \tag{12}$$

The static model in (12) can be expressed in a compact form by the introduction of two dimensionless parameters, given in (13):

$$\chi = \frac{r}{R}, \quad \lambda = -\frac{v_0}{\dot{\phi}R} \tag{13}$$

The ratio χ represents the span-ratio which is the position of a blade element with respect to the length of the blade. The ratio λ represents the tip-speed-ratio which is the relation of the vertical descent speed to the speed of the tip of the blade. The ratio λ/χ produces a local speed ratio which describes the relation of the local angular velocity of a blade element to the vertical descent speed of the entire samara. Inclusion of the local speed ratio provides insight into span-wise characteristics. Using the ratios in (13), we have the following expressions for the local $\|U_\infty\|$ and α under steady autorotation,

$$\begin{aligned}
\|U_\infty\|^2 &= r^2\dot{\phi}^2\cos^2\theta\left[1 + \left(\frac{\lambda}{\chi}\right)^2\right], \\
\sin\alpha &= (r\dot{\phi}\sin\psi - v_0\cos\psi)\cos\theta/\|U_\infty\|, \\
\cos\alpha &= (r\dot{\phi}\cos\psi + v_0\sin\psi)\cos\theta/\|U_\infty\|, \\
\Rightarrow \tan\alpha &= \left(\tan\psi + \frac{\lambda}{\chi}\right)/\left(1 - \tan\psi\frac{\lambda}{\chi}\right)
\end{aligned} \tag{14}$$

It should be noted here that for negligible ψ, the right hand side of (14) reduces to the local speed ratio of the blade element. Expanding (12) using (8), (9) and (14) produces the following system of equations:

$$\begin{aligned}
M_{y_3} &= -I_{y_3y_3}\dot{\phi}^2\sin\theta\cos\theta\cos\psi \\
&= -\frac{1}{2}\rho\dot{\phi}\cos^2\theta\int_{r_0}^{r_f} r^3\, w(r)\sqrt{1 + \left(\frac{\lambda}{\chi}\right)^2} \\
&\quad \left[\left(C_D(\alpha) - \frac{\lambda}{\chi}C_L(\alpha)\right)\sin\psi - \right. \\
&\quad \left.\left(C_L(\alpha) + \frac{\lambda}{\chi}C_D(\alpha)\right)\cos\psi\right]dr
\end{aligned} \tag{15}$$

Table 1. SAMARA AND ENVIRONMENTAL PARAMETERS

C_{D_0}	0.124	–
$I_{y_3y_3}$	1.26×10^{-8}	$kg\,m^2$
m	0.00013	kg
R	0.035	m
r_0	$0.2R$	m
r_f	$0.9R$	m
ρ	1.225	kg/m^3

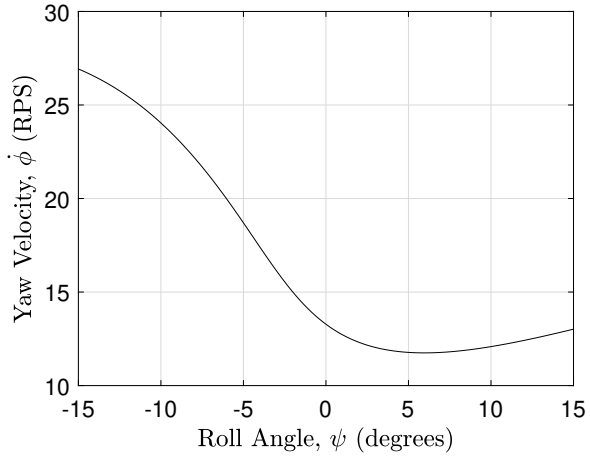

Fig. 3. Steady-state yaw velocity over range of roll angles

$$
\begin{aligned}
M_{z_3} =& I_{y_3y_3}\,\dot{\phi}^2 \sin\theta\cos\theta\sin\psi \\
=& \frac{1}{2}\rho\,\dot{\phi}\,\cos^2\theta \int_{r_0}^{r_f} r^3\,w(r)\sqrt{1+\left(\frac{\lambda}{\chi}\right)^2} \\
& \left[\left(C_L(\alpha)+\frac{\lambda}{\chi}C_D(\alpha)\right)\sin\psi + \right. \\
& \left.\left(\frac{\lambda}{\chi}C_L(\alpha)-C_D(\alpha)\right)\cos\psi\right] dr
\end{aligned} \tag{16}
$$

$$
\begin{aligned}
mg =& \frac{1}{2}\rho\,\dot{\phi}^2\,\cos^3\theta \int_{r_0}^{r_f} r^2\,w(r)\sqrt{1+\left(\frac{\lambda}{\chi}\right)^2} \\
& \left[C_L(\alpha)+\frac{\lambda}{\chi}C_D(\alpha)\right] dr
\end{aligned} \tag{17}
$$

Here a simplistic thin airfoil model is employed to select values for C_L and C_D, the coefficients of lift and drag, respectively, White (2011). Specifically,

$$
\begin{aligned}
C_L(\alpha) &= 2\pi\sin\alpha \\
C_D(\alpha) &= C_L(\alpha)\sin\alpha + C_{D_0}
\end{aligned} \tag{18}
$$

where C_{D_0} is a tuned additional drag coefficient to account for roughness and airfoil thickness. Equations (13), (15), (16) and (17) can be numerically solved for the steady-state values of $\dot{\phi}$, θ, v_0, and λ for a range of values of ψ.

5. STEADY-STATE RESULTS

Steady-state simulation was performed for the case of Acer plantanoides samaras to compare with experimental results provided in Norberg (1973). Physical parameters of the samara in question, as well as environmental properties used for the following simulation results are presented in Table 1.

As previously stated, the above steady-state model was produced for an arbitrary roll angle, ψ. This allows for simulation of a range of equilibrium results for a span of ψ values. Fig. 3 displays the variation of steady-state $\dot{\phi}$ with changing ψ inputs. It can be seen that the value of $\dot{\phi}$ at $\psi = 0$ is approximately 13.3 rev/s which agrees well with the value of 13 rev/s found in Norberg (1973). It can also be observed that significant error is introduced to the simulated value of $\dot{\phi}$ when a negative roll angle is applied. Figure 4 presents the angle of pitch, θ, taken by the samara at steady-state for the span of ψ. Not only does the value of $\theta = 20.0°$ at $\psi = 0$ agree with the 20° value

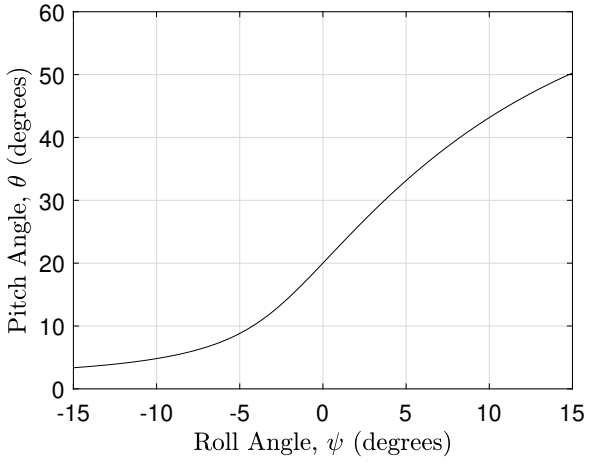

Fig. 4. Steady-state pitch angle over range of roll angles

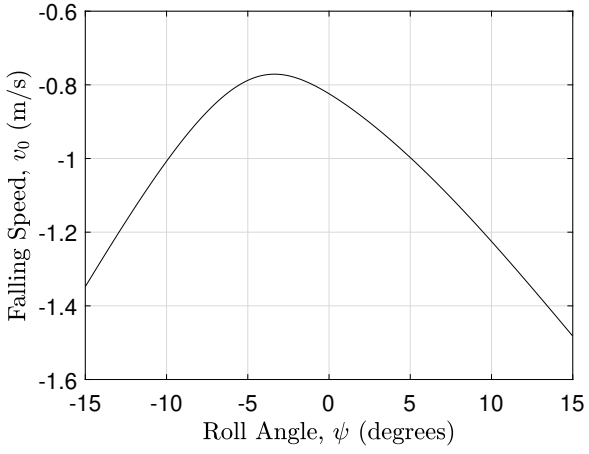

Fig. 5. Steady-state terminal velocity over range of roll angles

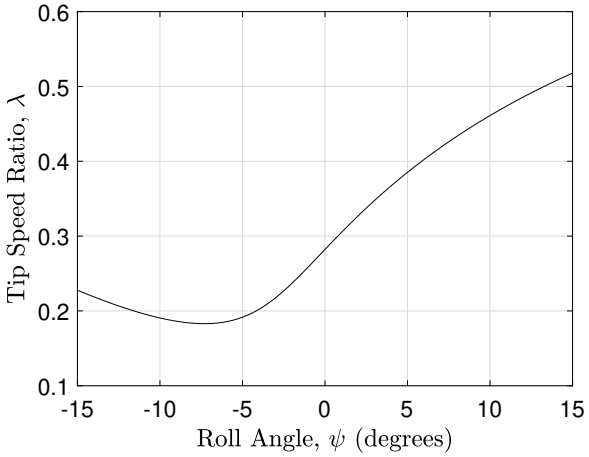

Fig. 6. Steady-state tip speed ratio over range of roll angles

reported in Norberg (1973), but it can be seen from the variation of the plot that even small changes in ψ produce significant error in the steady-state θ value. This supports the assumption that negligible roll is present at steady-state. Figure 5 presents the change in terminal velocity for the span of prescribed ψ values. The simulated terminal velocity of approximately 0.82 m/s (downwards) shows good agreement with the experimental value of 0.9 m/s reported in Norberg (1973).

It was observed that the accuracy of steady-state results is sensitive to small changes in C_L and C_D. This observation is in agreement with the claims of Rosen and Seter (1991). The addition of the C_{D_0} term provides a means of adjusting model accuracy to better represent the additional aerodynamic effects experienced in low Reynolds Number flight. The values of C_{D_0} and $I_{y_3y_3}$ presented in Table 1 were numerically optimized to better represent the Acer plantanoid samaras studied in Norberg (1973). The value of C_{D_0} selected from this process agrees well with literature for insect wings in low Reynolds Number conditions, as presented in Rosen and Seter (1991). It has been observed that for a samara with arbitrary curvature/warping, a minor improvement in steady-state modeling may be achieved at non-zero ψ values between $-0.6° < \psi < 0.6°$, however this deviation appears to be dependent on geometric variations, and thus is specimen-specific. Further investigation into this claim through experimentation will be presented in future work.

6. DYNAMICS SIMULATIONS

Expanding upon the presented model, the transient behavior of a falling samara is next studied through simulations. Steady-state analysis has shown that it is reasonable to assume $\psi = 0$ near equilibrium. It has been observed that a falling samara establishes autorotation in a matter of a few seconds. This coupled with the minuscule rolling moment of inertia, $I_{x_3x_3}$, suggests that achieving negligible roll angle will be nearly instantaneous. It is therefore reasonable for this reduced order model to extend the assumption of $\psi = 0$ to transients. For consistency with the steady-state analysis, ψ has been presented as a constant input. The resulting dynamic model is given in (10) and (11). Transient simulation results are presented in Figs.7-10. Case 1 (bold) shows the model response with all initial conditions set to 0 (i.e. $\{\theta\ \dot{\theta}\ \dot{\phi}\ v_0\} = \{0\ 0\ 0\ 0\}$). Case 2 (dashed) has initial conditions of $\theta = 45°$, $\dot{\theta} = 0.175$ rad/s, $\dot{\phi} = 4$ rev/s, and $v_0 = -0.4$ m/s.

Figure 7 displays the pitch response, θ, of the samara for both cases. An aggressive stabilization is observed, showing an initial overshoot before smoothing out at approximately 0.5 seconds. The following smooth dynamic settles into steady autorotation in a matter of 1 second. A similar behavior is observed in Figs.8, 9, and 10 which present the response of the rate of pitch, $\dot{\theta}$, rate of yaw, $\dot{\phi}$, and vertical velocity, v_0, respectively. An initial phase of oscillation can be seen in the $\dot{\theta}$ response of Fig. 8. In both cases, the amplitude of $\dot{\theta}$ oscillation decays after 2 peaks to assume a smooth trend which approaches 0 at steady-state. Special attention should be given to the response of v_0 where it can be seen that the value at approximately 0.25 seconds is characteristic of maximum

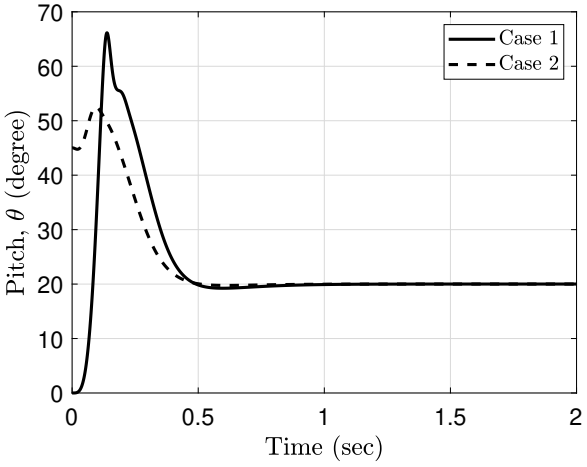

Fig. 7. Dynamic pitch response

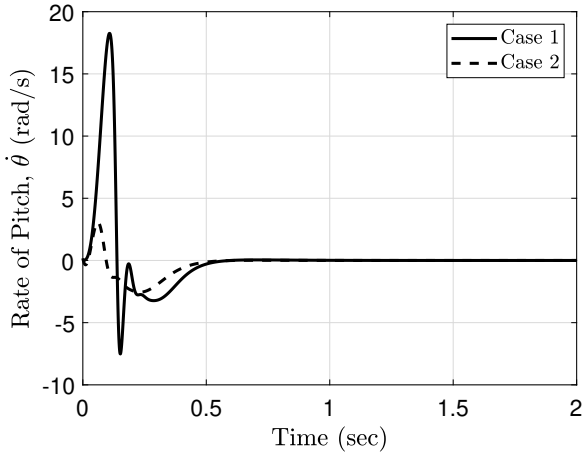

Fig. 8. Dynamic rate of pitch response

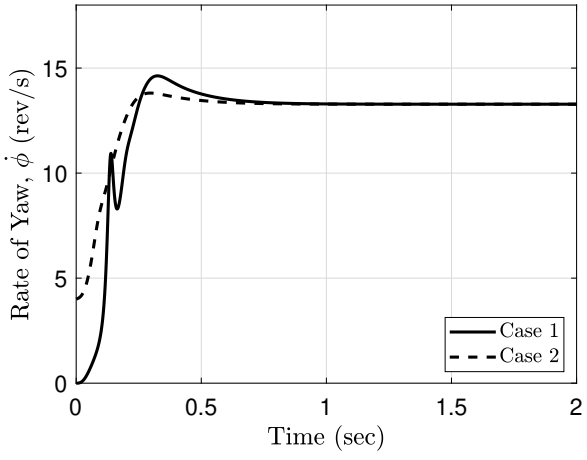

Fig. 9. Dynamic yaw response

descent speed. Past this point, the samara slows to its autorotative terminal velocity. The steady values of the dynamic simulation show complete agreement with those of the steady state model, as expected.

The equilibrium of autorotation can be viewed as a balancing of counteracting yawing moments along the span of a rotor-craft blade. This effect is visualized in Fig. 11 which displays the moment provided by each blade element of a samara. For the presented case (Case 1), the entire blade provides a moment to increase the rotation of the samara. This effect reduces over time until steady state is

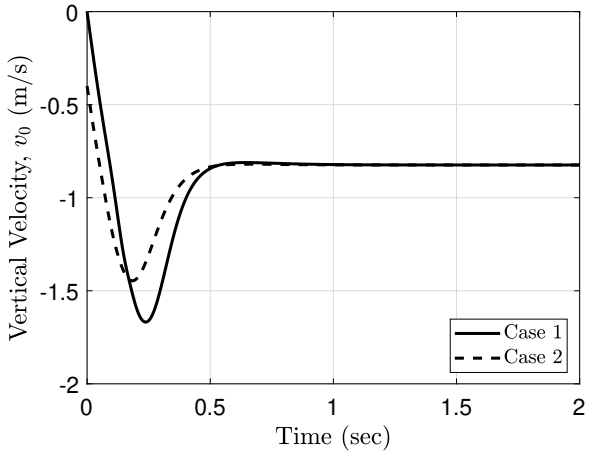

Fig. 10. Vertical velocity dynamic response

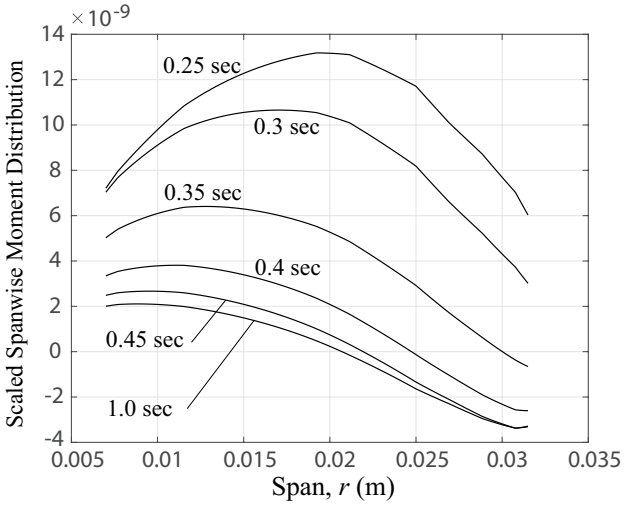

Fig. 11. Scaled yawing moment along span of the blade (Case 1)

reached. It can be seen that at 1 seconds an approximately equal region of positive and negative moment is present, suggesting equilibrium. This result agrees with the predicted performance of helicopter blades in autorotation, Leishman (2006).

Observation of samaras found in nature and simulation of the presented model from various initial conditions has suggested the autorotational equilibrium of a single-winged samara is characterized by a large region of attraction. Stability investigation of the equilibrium is a topic of interest and future research for the authors.

7. CONCLUSION

A simplified and compact model for the steady-state behavior of a single winged samara has been presented. It has been shown that an assumption of negligible roll angle, $\psi = 0°$, can be made to produce steady-state equilibria in agreement with experimental data. Extending to a dynamic representation, a reduced order model under the assumption of $\psi = 0°$ produces reasonable transient behavior and equivalent steady-state results. The stablization of the reduced order samara model has been visualized for two different initial conditions. Ongoing and future work in continuation of this research include model refinement, experimentation, as well as linear and nonlinear stability analysis.

REFERENCES

Augspurger, C. (1986). Morphology and dispersal potential of wind-dispersed diaspores of neotropical trees. *American Journal of Botany*, 73(3), 353–363.

Augspurger, C. and Franson, S. (1987). Wind dispersal of artificial fruits varying in mass, area, and morphology. *Ecology*, 68(1), 27–42.

Burrows, F. (1975). Wind-borne seed and fruit movement. *New Phytologist*, 75, 405–418.

Green, D. (1980). The terminal velocity and dispersal of spinning samaras. *American Journal of Botany*, 67(8), 1218–1224.

Green, D. and Johnson, E. (1990). The aerodynamics of plumed seeds. *Functional Ecology*, 4, 117–125.

Green, D. and Johnson, E. (1993). Seed mass and dispersal capacity in wind-dispersed diaspores. *OIKOS*, 67, 69–74.

Hertel, H. (1966). *Structure Form and Movement*. Reinhold Publishing Corporation, New York, NY.

Holden, J. (2016). *Experimental Testing and Computational Fluid Dynamics Simulation of Maple Seeds and Performance Analysis as a Wind Turbine*. Master's thesis, University of Cincinnati, Cincinnati, Ohio.

Leishman, J.G. (2006). *Principles of HELICOPTER AERODYNAMICS*. Cambridge University Press, New York, NY, second edition.

Lentink, D., Dickson, W., van Leeuwen, L., and Dickson, M. (2009). Leading-edge vortices elevate lift of autorotating plant seeds. *SCIENCE*, 324, 1438–1440.

Limacher, E. (2015). *Samara-Seed Aerodynamics*. Master's thesis, University of Calgary, Calgary, Alberta.

Nathan, R., Safriel, U., Noy-Meir, I., and Schiller, G. (1996). Samara's aerodynamic properties in pinus halepensis mill., a colonizing tree species, remain constant despite considerable variation in morphology. *Preservation of Our World in the Wake of Change*, VI A/B, 553–556.

Norberg, R. (1973). Autorotation, self-stability, and structure of single-winged fruits and seeds (samaras) with comparative remarks on animal flight. *Biological Review*, 48, 561–596.

Rosen, A. and Seter, D. (1991). Vertical autorotation of a single-winged samara. *Journal of Applied Mechanics*, 58, 1064–1071.

Seter, D. and Rosen, A. (1992). Stability of the vertical autorotation of a single-winged samara. *Journal of Applied Mechanics*, 59, 1000–1008.

Ulrich, E., Humbert, J., and Pines, D. (2010). Pitch and heave control of robotic samara micro air vehicles. *Journal of Aircraft*, 47, 1290–1299.

Ulrich, E. and Pines, D. (2012). Effects of planform geometry on mechanical samara autorotation efficiency and rotational dynamics. *Journal of the American Helicopter Society*, 57, 012003.

White, F.M. (2011). *FLUID MECHANICS*. McGraw-Hill, New York, NY, seventh edition.

Yasuda, K. and Azuma, A. (1997). The autorotation boundary in the flight of samaras. *Journal of Theoretical Biology*, 185, 313–320.